Article

Dynamic Simulation of an Absorption Cooling System with Different Working Mixtures

Jesús Cerezo [1,*] [iD]**, Rosenberg J. Romero** [1] [iD]**, Jonathan Ibarra** [1] [iD]**, Antonio Rodríguez** [1]**, Gisela Montero** [2] [iD] **and Alexis Acuña** [2] [iD]

[1] Centro de Investigación en Ingeniería y Ciencias Aplicadas, Universidad Autónoma del Estado de Morelos, Av. Universidad 1001, Cuernavaca 62209, Morelos, Mexico; rosenberg@uaem.mx (R.J.R.); jibarra@uaem.mx (J.I.); antonio_rodriguez@uaem.mx (A.R.)

[2] Universidad Autónoma de Baja California, Blvd. Benito Juárez y Calle de la Normal S/N, Insurgentes Este, Mexicali 21280, Baja California, Mexico; gmontero@uabc.edu.mx (G.M.); alexis.acuna@uabc.edu.mx (A.A.)

* Correspondence: jesus.cerezo@uaem.mx; Tel.: +52-777-329-7000

Abstract: High consumption of electricity represents an economic and social problem in warm places, caused by the massive use of cooling machines. Absorption systems are a sustainable method for air conditioning applications. However, environmental conditions should be analyzed to avoid crystallization problems of the working mixture. This article presents a thermal analysis of a solar absorption cooling system in dynamic conditions using NH_3-H_2O, H_2O-LiBr, NH_3-NaSCN, NH_3-$LiNO_3$, and H_2O-LiCl working mixtures using Equation Engineering Solver (EES) and TRaNsient SYstem Simulation (TRNSYS) software. A solar collector area of 42.5 m^2 was selected to carry out the thermal analysis. The results showed that H_2O-LiCl obtained the maximum solar (0.67) and minimum heating (0.33) fraction. However, it obtained the maximum lost heat fraction (0.12), in spite of obtaining the best coefficient of performance (COP) among the other working mixtures, due mainly to a crystallization problem. The gain fraction (GF) parameter was used to select the adequate solar collector number for each working mixture. NH_3-$LiNO_3$ and NH_3-H_2O obtained the highest GF (up 6), and both obtained the maximum solar (0.91) and minimum heating (0.09) fraction, respectively, using 88.8 and 100.4 m^2 of solar collector area, respectively.

Keywords: solar absorption cooling; evacuated tube solar collector; dynamic condition; crystallization

1. Introduction

Cities located in warm places have a high consumption of electricity, especially in the summertime. This is a socio-economic and environmental problem that is due to the use of air conditioning and refrigeration. They are largely based on the consumption of non-renewable primary resources.

Solar-powered absorption cooling systems use solar heat to drive an absorption chiller and produce a cooling effect in a sustainable way; however, some working mixtures have crystallization problems depending on the changes in environmental temperature, and this is the main problem for these devices because it blocks the internal pipes and stops the chiller operation [1].

In the literature, there are some studies about absorption cooling systems (ACS) in dynamic conditions: Ahmed et al. [2] carried out a simulation based on a performance analysis of a solar assisted single effect absorption cooling system for two system configurations in TRaNsient SYstem Simulation (TRNSYS). In configuration 1 (C-1), the working fluid returning from the generator of the absorption chiller flows toward the hot storage tank. In configuration 2 (C-2), the working fluid returning from the absorption chiller may become isolated from the collector-storage tank loop if the fluid temperature in the storage tank is inferior to the required temperature and is directly fed to the

auxiliary boiler. The results showed that C-2 resulted in higher energy saving than C-1 for the whole summer season.

Stanciu et al. [3] analyzed an NH_3-H_2O absorption cooling system driven by solar energy. A fully mixed hot water storage tank was used to provide the thermal energy to the generator from the heat collected by a fixed oriented parabolic trough collector. According to the author's results, for the longest continuous operation of the NH_3-H_2O cooling system (from 09:00 to 17:10) 10 m × 2.9 m parabolic trough collector (PTC) aperture dimensions with a 0.16 m^3 storage tank volume were calculated at 10 °C of evaporator temperature. In the same year, Stanciu et al. [4] simulated a solar driven cooling system consisting of a single effect H_2O-LiBr absorption cooling system, a parabolic trough collector, and a storage tank module was analyzed for one full operation day. The simulation was constrained to operate at the maximum exergetic efficiency of the absorption system, under a time-dependent cooling load. A constant evaporator of 10 °C was considered. To set up the solar assembly, two commercial PTCs were selected, namely PT1-IST and PTC 1800 Solitem. The results showed that the best choice for the studied case was the use of two commercial PTC 1800 collectors connected in series with a modular storage tank with capacities of 90 and 140 kg. The simulation incorporated the fact that the system operates continuously between 09:00 to 18:00 on a calm day (0.2 m/s wind velocity). On a windy day (considering a wind speed of 5 m/s), the computations revealed that the operation time interval was reduced to 09:00 to 17:40 due to important energy losses in the PTC.

Sokhansefat et al. [5] carried out a parametric analysis to find the optimum configuration for a 5-ton capacity solar absorption system in transient conditions using TRNSYS software in Tehran. The results indicated that the performance of the setup is capable of 28% enhancement. The optimum values were a collector area of 55 m^2, storage tank volume of 1 m^2, temperature set point of the auxiliary boiler of 77 °C, solar collector mass flow rate at 1000 kg/h, and collector slope of 33°.

Antonopoulos and Rogdakis [6] studied the performance of absorption heat pumps using NH_3-$LiNO_3$ and NH_3-NaSCN in Atenas, Greece. The results showed that NH_3-$LiNO_3$ was better than NH_3-NaSCN for heating because it provides a higher heat-gain factor and useful thermal power. For cooling the NH_3-$LiNO_3$ system provides a higher cooling power, while NH_3-NaSCN achieves a higher coefficient of performance (COP).

Florides et al. [7] presented an H_2O-LiBr solar absorption cooling system simulation in TRNSYS software under typical conditions in Nicosia, Cyprus. That study consisted of optimizing the storage tank size, slope, and area of the parabolic solar collector. The results showed that the ideal size of the solar collector was 15 m^2 with an inclination of 30° and 600 L of the storage tank for the generation of 84,240 MJ. Arzoz et al. [8] presented a simulation of a double effect absorption cooling of 3 kW with NH_3-$LiNO_3$ using flat solar collectors in Madrid, Spain. The results showed that the equipment could operate about 6 hours of solar cooling at −15 °C, obtaining a COP of 0.3 at a condensation temperature of 40 °C of condensation temperature. The thermal fluid reached a maximum temperature of 100 °C with a solar efficiency of 0.27.

De Francisco et al. [9] carried out a test for the NH_3-H_2O absorption refrigeration system at 2 kW. The generated heat was dissipating by natural convection in the absorber and condenser components and the system was manually controlled. The results showed that the COP obtained was very low (0.05); however, the authors concluded that it could be improved using forced convection.

Assim et al. [10] modeled an absorption chiller operated by hot water using an evacuated tube collector in TRNSYS software. It was found that the use of a hot water storage tank and a 12 m^2 collector area were sufficient to maintain the room temperature at 26 °C or below during the cooling season. Agrouaza et al. [11] studied a solar cooling system in several cities of Morocco and it was found that Errachindia city obtained the best average annual solar fraction (30%) and a COP value of 0.33. The COP values varied from 0.12 to 0.33 all across the year in other regions.

The H_2O-LiBr and NH_3-H_2O are the conventional working mixtures used in commercial absorption systems due to advantages in their thermodynamic properties. H_2O-LiBr obtained

higher COP than the NH_3-H_2O system, though it has crystallization problems. The NH_3-$LiNO_3$ and NH_3-NaSCN systems are a suitable alternative to NH_3-H_2O and both have the advantage of working either refrigeration or air conditioning [12], even though the values of COP are a little higher than the NH_3-H_2O system at a high generator temperature. Recently Gogoi and Knowar [13] carried out an energetic and energetic comparison with H_2O-LiCl and H_2O-LiBr systems under a similar working condition. They concluded that H_2O-LiCl obtained a higher COP than the H_2O-LiBr system. However, H_2O-LiCl has crystallization problems that depend on environmental temperature changes. Table 1 shows a comparison of working mixtures.

Table 1. Comparative data among working mixtures.

Working Mixture	COP *1	T_{ACT} *2	Crystallization	Price *3 (USD)	Pressure (Bar)	Refrigeration Condition
H_2O-LiBr	0.80	low	medium	131.35 ($\geq$99.0 wt %)	vacuum	no
H_2O-LiCl	0.82	low	high	153.35 (>99.0 wt %)	vacuum	no
NH_3-H_2O	0.67	medium	no	193.45 (>99.9 wt %)	>10	yes
NH_3-$LiNO_3$	0.69	medium	medium	353.25 (>99.0 wt %)	>10	yes
NH_3-NaSCN	0.65	medium	medium	180.20 (>98.0 wt %)	>10	yes

*1 Operation condition: T_{GE} = 75 °C, T_{AB} = T_{CO} = 35 °C, T_{EV} = 8 °C; *2 T_{ACT} Activation temperature of the single stage absorption chiller; *3 Sigma-Aldrich, web page: www.sigmaaldrich.com.

Most papers published about the absorption cooling system mainly use only one working mixture in dynamic conditions. The objective of this paper was to carry out a thermodynamic analysis of an ACS using conventional (NH_3-H_2O and H_2O-LiBr) and unconventional (NH_3-$LiNO_3$, NH_3-NaSCN, and H_2O-LiCl) working mixtures based on the COP and the limitation on the crystallization of the solution for dynamic conditions.

2. Description of the System

The present study consists of the cooling of a building via a single stage absorption cooling system using evacuated solar collectors (SC) and an auxiliary system (AS), as shown in Figure 1. The auxiliary system is used to control the temperature coming from the solar collectors to the generator component (GE).
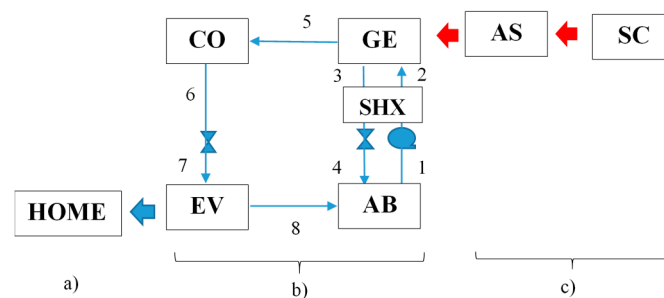

Figure 1. Diagram of the cooling system: (**a**) building; (**b**) absorption cooling system; and (**c**) solar collector and auxiliary system.

3. Simulation of the Solar Cooling System

The TRNSYS [14] software was used to simulate the solar absorption system for the cooling of a building located in Temixco City, Mexico. Figure 2 shows the schematic diagram of the process. There are two main circuits: solar collector (red line) and cooling (blue line). In the solar collector circuit, heating fluid (water) is pumped (Type 3d) from a storage tank (Type 4a) into the evacuated solar collector (Type 1b) and returned to the tank. This pump is controlled by Type 2b and it is turned on when the output is higher than the input temperature of the solar collector; otherwise, it is turned off. In the cooling circuit, a heating fluid is sent to the auxiliary system (Type 66a) to control the supply

temperature and enter towards to the generator component of the absorption cooling system (Type 66a-2). Finally, it is pumped by Type 3d-2 to the tank. The pump Type 3d-2 is controlled by Type 2b-2 and it is turned on when the building cooling load (Type 56) was activated to keep an indoor temperature below 25 °C. Type 66a and Type 66a-2 are programmed in Equation Engineering Solver (EES [15]) and both are coupled with the TRNSYS model for an hourly simulation.
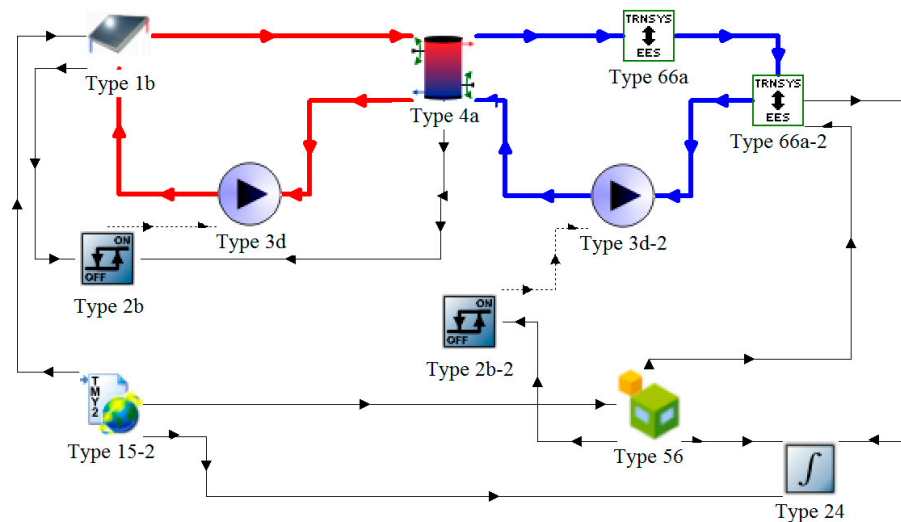

Figure 2. Diagram of the solar cooling system in TRaNsient SYstem Simulation (TRNSYS).

The TRNSYS software has incorporated modules (types) to model a single-effect absorption chiller from normalized data from catalogs of the manufacturer. However, NH_3-$LiNO_3$, NH_3-$NaSCN$, and H_2O-$LiCl$ are still not available. Therefore, it was necessary to develop the mathematical model for each working mixture to simulate the ACS (Appendix A presents the basic equations, suppositions, and validation). The interaction between the Type 66a-2 and Type 56 consisted in: the instant cooling capacity of the building is equal to the evaporator component of the ACS. The operation of the ACS incorporated a heat transfer in the generator component of $\Delta T = 5$ °C between the supply and generator temperatures ($T_{SUPPLY} = T_{GE} + 5$ °C) using water as the heating fluid. The heat transfer between the environment, and the condenser and absorber components involved a $\Delta T = 10$ °C ($T_{CO} = T_{AB} = T_{ENV} + 10$ °C) cooled by air.

Type 66a is the auxiliary system and it was used to control the supply temperature to the ACS by using a heating (Q_{HS}) or dissipating (Q_{DS}) system.

The solar thermal collector efficiency (Type 1b) was calculated using a quadratic or linear efficiency equation according to ASHRAE or European standards. The solar collector is an HTP-Evacuated Tube HP-30SC [16] with a net aperture area of 3.86 m². The cover is made of a glass vacuum tube and the absorber material is made of tube-copper and steel/plate-glass, with a tilt angle of 19° (corresponding to the location latitude). The solar thermal collector efficiency is presented in Equation (1) [16],

$$\eta = 0.418 - 1.17 \frac{(T_{IN} - T_{ENV})}{Q_{RAD}} \tag{1}$$

where T_{IN} and T_{ENV} are the input temperatures of the solar collector and environment temperature, respectively, and Q_{RAD} is the global radiation incident (W/m² °C).

The Type 56 is a multi-zone building with 4 windows and only one zone, with some dimensions and main building characteristics shown in Table 2. Four occupants in a rest position and three computers turned on from 08:00 to 18:00 were considered as heat generation.

Table 2. Building characteristics.

Concept	Quantity
North and south wall	$35\ \text{m}^2$
Ceiling and floor	$75\ \text{m}^2$
West and east wall	$12.5\ \text{m}^2$
Thickness of walls	0.12 m brick
Windows	$1\ \text{m}^2$
Air change of ventilation	$6\ \text{h}^{-1}$

The Type 4a is a stratified storage tank. The properties and working conditions supplied were: a heat capacity of 4.19 kJ/kg K, a height of 1 m, an initial temperature of 70 °C, and a loss coefficient = 0.75 W/m² K. The characteristics of the thermal insulation are: density = 16 kg/m³, thickness = 0.05 m and, thermal conductivity = 0.05 W/m K.

4. The Mathematical Model of the Solar Cooling System

4.1. Assumptions

- The pressure drops and heat losses are negligible for each pipeline.
- Fraction pump power (The energy converted to fluid thermal energy, fpar) was 0.05.

4.2. Basic Equation (Energy and Mass Balances)

This section presents a brief mathematical description [17] for each component model (Types).

The pump (Type 3d) computes a mass flow rate using a variable control function ($0 \leq \gamma \leq 1$) and a fixed (user-specified) maximum flow capacity (m_{MAX}).

$$m_{IN}\ C_P\ (T_{OUT} - T_{IN}) = P\ \text{fpar} \tag{2}$$

$$m_{OUT} = \gamma\ m_{MAX} \tag{3}$$

where fpar is the fraction pump power, p is the power (kW), m_{OUT} is the output mass flow rate (kg/s) and, C_p is the heat capacity of the fluid (kJ/kg K).

The solar collector (Type 1b) uses a general equation for solar thermal collector efficiency (η) and it is calculated via Equations (4) and (5),

$$\eta = \frac{Q_U}{AQ_{RAD}} = \frac{mC_p(T_{OUT} - T_{IN})}{AQ_{RAD}} \tag{4}$$

where Q_U is the useful heat of the solar collector (W), A is the gross area (m²) and, Q_{RAD} is the global radiation incident on the solar collector (W/m²). Equation (4) can be rewritten as:

$$\eta = a_0 - a_1 \frac{(T_{IN} - T_{ENV})}{Q_{RAD}} - a_2 \frac{(T_{IN} - T_{ENV})^2}{Q_{RAD}} \tag{5}$$

where the constants a_0, a_1 and a_2 are, respectively, the intercept of the collector efficiency, the negative of the first-order coefficient and the negative of the second-order coefficient. The quadratic Equation (5) can be written as a linear Equation (1) with very similar results.

The stratified storage tank (Type 4a) can be modeled by assuming that the tank consists of N fully-mixed equal volume segments. An energy balance written in the ith tank segment (i) is expressed as:

$$m_i C_{p,f} \frac{dT_i}{dt} = \alpha_i m_h C_{p,f}(T_h - T_i) + \beta_i m_L C_{p,f}(T_L - T_i) + UA_i(T_{ENV} - T_i) \tag{6}$$

where m, T, and t are the mass flow rate, temperature and time, respectively. Subscripts h, L, and f are the solar collector, cooling auxiliary circuits and fluid, respectively (see Section 3), α_i and β_i are a control function, and U is the loss coefficient between the tank and its environment (kW/m^2 °C).

The Quantity integrator (Type 24) integrates a series of quantities over a period of time using the following equation,

$$Y_i = \int X_i dt \tag{7}$$

where X_i is the ith quantity to be integrated and Y_i is the time integral of X_i

The multizone building (Type 56) models the thermal behavior of a building having multiple thermal zones, with the thermal capacity of the air volume and capacities which are closely connected with the air node (see Figure 3a). The convective heat that flows to the air node is calculated using Equation (8).

$$Q_i = Q_{suf,i} + Q_{inf,i} + Q_{vent,i} + Q_{ic,i} + Q_{af,i} + Q_{solar,i} + Q_{asr,i} \tag{8}$$

$$Q_{surf,i} = h_i A (T_{surface,i} - T_{air}) \tag{9}$$

$$Q_{inf,i} = V\rho C_p (T_{outside,i} - T_{air}) \tag{10}$$

$$Q_{vent,i} = V\rho C_p (T_{ventilation,i} - T_{air}) \tag{11}$$

$$Q_{af,i} = V\rho C_p (T_{zone,i} - T_{air}) \tag{12}$$

where the subscripts surf, inf, vent, ic, af, solar and asr are the energy gain for convective heat due to the: surfaces, infiltration (air flow from the outside only), ventilation (user-defined air flow), internal convective heat (people, equipment, radiator, etc.), the air flow from air node i or boundary condition, the fraction of solar radiation (due to the external windows) and the absorbed solar radiation on all internal shading devices that is directly transferred as a convective gain to the internal air, respectively.
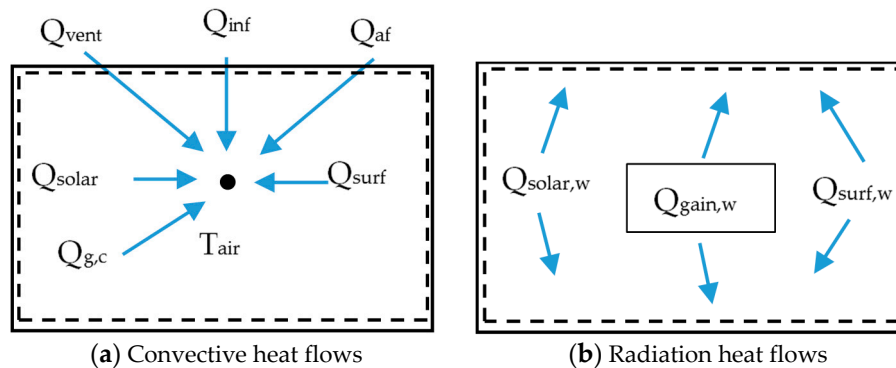

(**a**) Convective heat flows   (**b**) Radiation heat flows

Figure 3. Heat flows in the building; (**a**) due to the convective heat; (**b**) due to the radiation.

The radiative heat flowing through the wall and window is calculated via Equation (13) (see Figure 3b),

$$Q_{w,i} = Q_{surf,w,i} + Q_{solar,w,i} + Q_{long,w,i} + Q_{gain,w} \tag{13}$$

where $Q_{w,i}$ represents the radiative gains for the wall surface temperature node, $Q_{surf,w,i}$ represents the radiative air node internal gains received by the wall, $Q_{solar,w,i}$ represents the solar gains through the zone windows received by the walls, $Q_{long,w,i}$ represents the longwave radiation exchange between this wall and all the other walls and windows, and $Q_{gain,w}$ represents the user-specified heat flow to the wall or window surface. All of these quantities are given in kW.

The auxiliary system (Type 66a) is used to control the supply temperature (T_{SUPPLY}), when the storage tank temperature (T_T) is lower than T_{SUPPLY} (obtained from Table 3); the heating system (Q_{HS})

is activated using a simple energy balance (Equation (14)); otherwise, the dissipation system (Q_{DS}) is activated and Equation (15) is applied to it:

$$Q_{HS} = m \, C_p \, (T_T - T_{SUPPLY}) \tag{14}$$

$$Q_{Ds} = m \, C_p \, (T_{SUPPLY} - T_T) \tag{15}$$

Table 3. Operation range of the supply temperature range for absorption cooling system (ACS).

$T_{CO} = T_{AB}$, °C	<35	<38	<40	<42	<43	<44
T_{SUPPLY}, °C (NH_3-H_2O)	73–135	80–135	85–135	90–135	93–135	96–135
T_{SUPPLY}, °C (NH_3-$LiNO_3$)	70–35	76–135	81–135	85–135	86–135	90–135
T_{SUPPLY}, °C (NH_3-NaSCN)	73–114	80–121	85–126	90–129	93–132	95–133
T_{SUPPLY}, °C (H_2O-LiBr)	72–90	78–96	83–100	87–103	90–106	92–107
T_{SUPPLY}, °C (H_2O-LiCl)	71–74	77–81	82–85	86–88	88–90	91–92

The Differential controller (Type 2b) is an on/off differential controller that, can have a value of 1 or 0. The value of the control signal is chosen as a function of the difference between upper (Th) and lower (Tl) temperatures, and both are compared with two dead-band temperature differences ΔTh and ΔTl. The new value of the control function depends on the value of the input control function at the previous time step.

The weather data processor (Type 15-2) serves the purpose of reading data at regular time intervals from an external weather data file, interpolating the data at time steps of less than one hour, and making it available for other TRNSYS components.

4.3. Numerical Procedure

The TRNSYS library includes many of the components commonly found in thermal and electrical energy systems, as well as component routines to handle input of weather data or other time-dependent forcing functions and output of simulation results. The default solver uses successive substitutions in order to solve the systems equations. The iterative numerical methods are based on a guess or initial values that are used as starting points for the iterations. If the system's equating is very complex it needs a good guess value [17].

EES software uses a variant of Newton's method [18] to solve systems of non-linear algebraic equations. The Jacobian matrix needed in Newton's method is evaluated numerically at each iteration. Sparse matrix techniques are employed to improve calculation efficiency and permit rather large problems to be solved in the limited memory of a microcomputer. The efficiency and convergence properties of the solution method are further improved by the step-size alteration and implementation of the blocking algorithm which breaks the problems into a number of smaller problems which are easier to solve. Several algorithms are implemented to determine the minimum or maximum value of a specified variable.

EES software supports Dynamic Data Exchange (DDE) commands in order to exchange information with other programs. DDE is a method of sending information to other programs through the Microsoft Windows operating system. Type 66 makes use of DDE commands to launch EES, pass parameter and input information to EES, and ask EES to solve and recuperate output information, which is then treated like the output from any other TRNSYS component [17].

5. Operation Range of the Auxiliary System (AS)

An analysis of the environment temperature was carried out in order to select the time of operation of the absorption cooling system (ACS). Type 15-2 was built in the TRNSYS software to simulate a year's environmental conditions obtained from meteorological data in Temixco city, Mexico. Figure 4

shows the environment temperature and global radiation profiles across a year. The period from March to May (1460–3560 h) was selected to operate the absorption system due to the highest ambient temperature in a year (blue box). The maximum and minimum environment temperatures were 16.3 and 33.5 °C, these conditions will be used to dissipate the heat load in the condenser and absorber components of the ACS. It is a limitation of the working operation because ACS could fall into the crystallization zone or low COP depending on the environmental temperature. COP is defined as the ratio of the energy absorbed in the evaporator to the energy supplied by the generator.
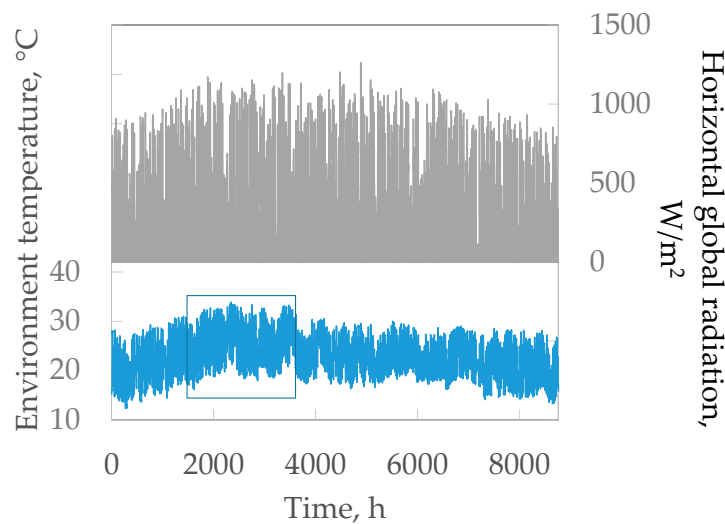

Figure 4. Environment temperature behavior along a year.

Figure 5 shows the minimum and maximum condenser and absorber temperatures that ACS will operate across the 3 months at 8 °C of the evaporator temperature. H_2O-LiCl obtained the highest COP (around 0.80–0.85) at T_{CO} = T_{AB} = 30 °C and NH_3-H_2O obtained the lowest COP value (lower than 0.70). On the other hand, H_2O-LiBr obtained the highest COP (around 0.73) and NH_3-H_2O the lowest value (lower than 0.53) at T_{CO} = T_{AB} = 44 °C. It is clear that the increment of T_{CO} and T_{AB}, decrease in the range of operation of ACS, mainly in the case of H_2O-LiCl, and range of operation of the generator temperature is from 55 to 69 °C (ΔT = 14 °C) and from 86 to 87 °C (ΔT = 1 °C) at a T_{CO} = T_{AB} of 30 and 44 °C, respectively.
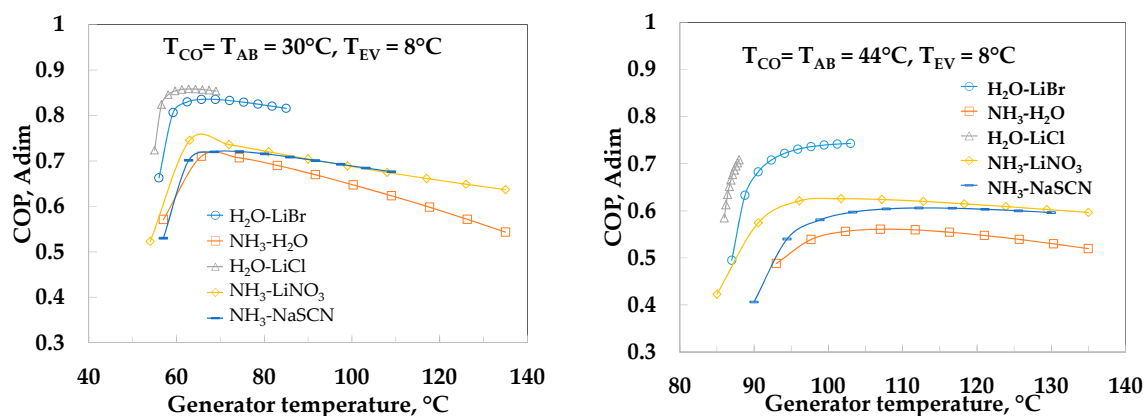

Figure 5. The coefficient of performance as a function of the generator temperature of an absorption cooling system.

The NH_3-$LiNO_3$ and NH_3-$NaSCN$ system obtained similar COP values; however, NH_3-$LiNO_3$ has a wider operating range than the NH_3-$NaSCN$ system. Both mixtures obtained a COP of around 0.68 to 0.72 and 0.60 to 0.63 at $T_{CO} = T_{AB} = 30$ and 44 °C, respectively.

Figure 6 shows the temperature as a function of the solution mass fraction for the absorber input, which is one of the streams most susceptible to fall in the crystallization zone (Point 4, from Figure 1b) corresponding to the same working condition in Figure 5. Crystallization temperatures are obtained mainly when the generator temperature obtained the maximum values; this means that the limit generator temperature is 82° at $T_{CO} = T_{AB} = 30$ °C in the case of the H_2O-$LiBr$ that corresponds to a 0.67 mass fraction and to 45 °C (Figure 6) located next to the crystallization line, as shown in Figure 7.
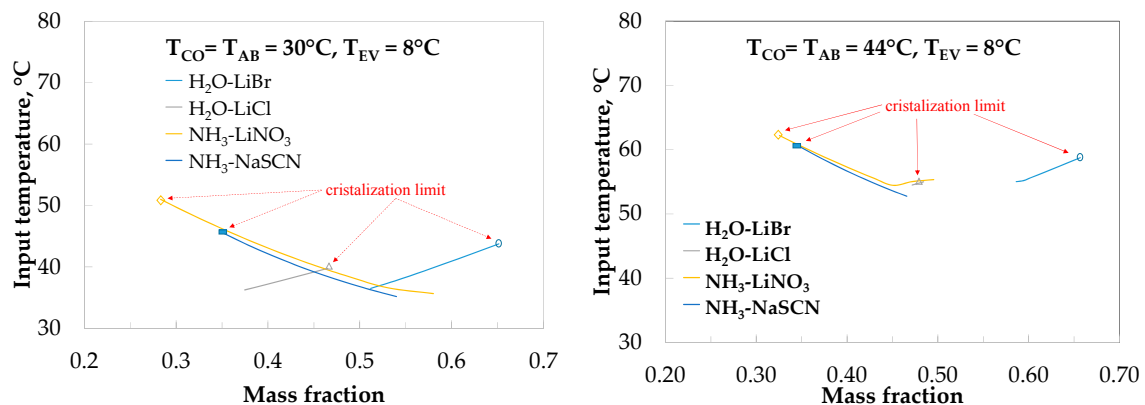

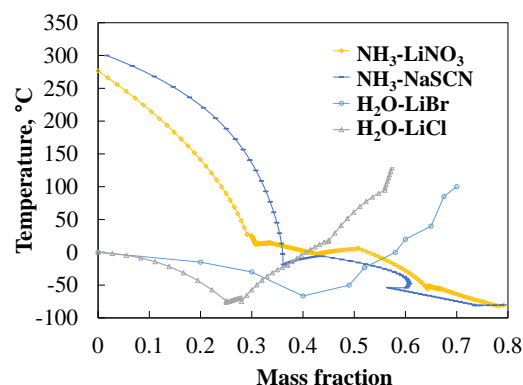**Figure 6.** Temperature and solution concentrations for the absorber's input.

Figure 7. Crystallization curves for several working mixtures.

Note that the mass fraction for H_2O-$LiBr$ and H_2O-$LiCl$ are defined as the ratio of the mass of the absorbent to the mass of the solution, and NH_3-$LiNO_3$ and NH_3-$NaSCN$ are defined as the ratio of the mass of the refrigerant (NH_3) to the mass of the solution.

The Auxiliary system (Type 66a) controls the supply temperature of the ACS in a dynamic way because the storage tank (T) and environment temperatures change throughout the day. When the supply temperature (see Table 3) was lower than the operation range, a heating system (Q_{HS}) is turned on, when it was higher than operation range it is turned off and the dissipating heat system (Q_{DH}) is turned on. Table 3 shows the operation range of the supply temperature in order to obtain COP values of up to 0.4 or in order to avoid falling into the crystallization zone for each working mixture.

It was necessary to work at several ranges when working in the generator temperature because a wider temperature range limits its function due to the crystallization (except the NH_3-H_2O system); besides, 135 °C was fixed as the maximum supply temperature.

6. Simulation Results

The total cooling energy consumption of the building was 1.43×10^7 kJ evaluated during 3 months, fixing a maximum indoor temperature of 25 °C. This value was calculated using Type 24, which integrates the instant cooling capacity over the time interval of the summary. Figure 8 shows the behavior of indoor and environment temperatures and the cooling capacity from 2000 to 2160 h (one week); as can be seen the cooling capacity was turned off when the indoor temperature was lower than 25 °C.
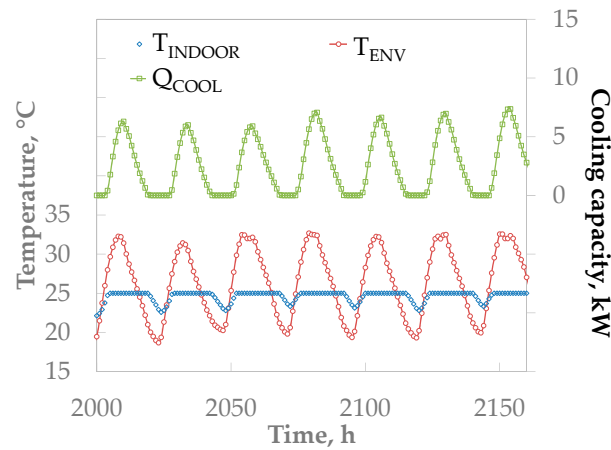

Figure 8. Indoor temperature and cooling capacity of the building.

The fractions of solar collector (SF), heating (HF), lost heat (LF) and Gain (GF) were the parameters we selected to compare each working mixture systems. They were defined in Equations (16)–(19) respectively.

$$SF = Qt_{SC}/Qt_{IN} \tag{16}$$

$$HF = Qt_{HS}/Qt_{IN} \tag{17}$$

$$LF = Qt_{LH}/Qt_{IN} \tag{18}$$

$$GF = Qt_{SC}/(Qt_{HS} + Qt_{LH}) \tag{19}$$

Qt_{IN} is the total energy input to the system due to the solar collectors (Qt_{SC}) and heating system (Qt_{HS}). Qt_{LH} is the lost heat caused by the dissipating heat system (Qt_{DH}) and the storage tank (Qt_T).

Figure 9 shows the number of solar collectors as a function of energy fractions, fixing a storage tank volume of 2 m^3 and a flow rate of 1000 kg/h for pumps P_1 and P_2. A collector area of 42.5 m^2 (11 solar collectors) was selected to compare each absorption system because this is the minimum number to satisfy the adequate relationship between the solar and heating fraction for all working mixtures. Note that the H_2O-LiCl system can be satisfied using 30 m^2 of collector area. Moreover, the lost heat fraction (red line) has a constant value around 0.07 for all working mixtures with few solar collector areas. It was caused by the energy loss from the storage tank; however, when the solar collector is increased, the LF increases significantly, mainly for H_2O-LiBr and H_2O-LiCl systems, and this is because the dissipating heating system is activated.
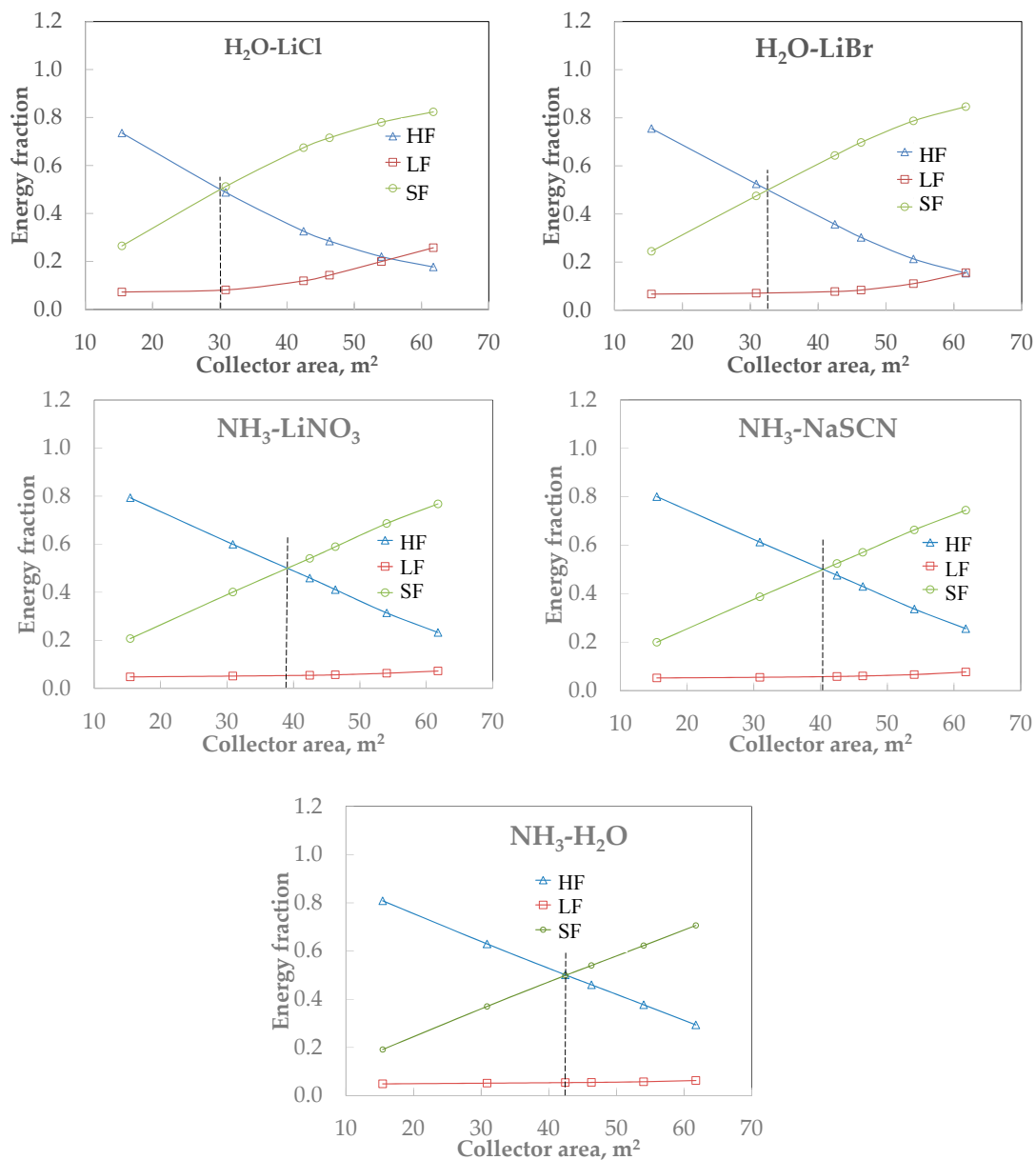
Figure 9. Energy fractions for each working mixture.

Figure 10 shows the COP behavior for each working mixture across one week from using 11 solar collectors (42.5 m^2); as can be seen the H$_2$O-LiCl system obtained the highest COP value (around 0.78–0.86), H$_2$O-LiBr obtained 0.70–0.83 and the NH$_3$-LiNO$_3$, NH$_3$-NaSCN and NH$_3$-H$_2$O systems obtained around 0.50–0.71.

Table 4 shows a resume of energy fractions evaluated over 3 months. The numbers that appear on the left side mean the best (1) and the worst (5) condition values. H$_2$O-LiCl obtained the maximum solar (0.67) and minimum heating (0.33) fraction; however, it obtained the maximum (0.12) lost heat fraction. This last value means that 12% of the energy supplied (Q$_{IN}$) was lost in the storage tank and the dissipating heat system. Note that SF + HF = 1.

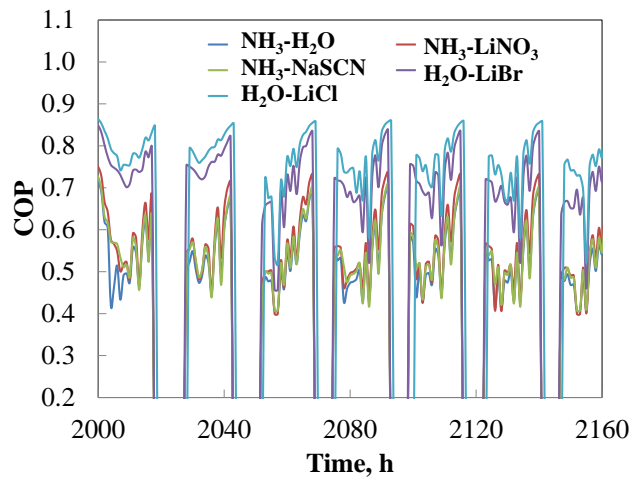**Figure 10.** The coefficient of performance as a function of time.

Table 4. Resume of energy fractions for all working mixtures.

Working Mixture	Solar Collector Area	SF	HF	LF
H_2O-LiCl	42.5	(1) 0.67	(1) 0.33	(5) 0.12
H_2O-LiBr	42.5	(2) 0.64	(2) 0.36	(4) 0.08
NH_3-$LiNO_3$	42.5	(3) 0.54	(3) 0.46	(1) 0.05
NH_3-NaSCN	42.5	(4) 0.52	(3) 0.48	(3) 0.06
NH_3-H_2O	42.5	(5) 0.50	(5) 0.50	(1) 0.05

Table 5 shows the total energy of the solar collector (Qt_{SC}), heating (Qt_{HS}), storage tank ($Qt_{LH,T}$) and dissipation heat ($Qt_{LH,D}$) evaluated during 3 months for each working mixture using 42.5 m^2 of collector area. The NH_3-$LiNO_3$ system obtained the maximum value of energy from solar collectors (2.13×10^7 kJ) and the H_2O-LiBr system was the worst (2.04×10^7 kJ). It was caused because the H_2O-LiBr system obtained a better COP value than the NH_3-$LiNO_3$ system; therefore, the storage tank temperature starts to increase, reducing the solar collector efficiency.

Table 5. Total energy using 11 solar collectors (42.5 m^2).

Working Mixture	Qt_{SC} (kJ)	Qt_{HS} (kJ)	$Qt_{LH,T}$ (kJ)	$Qt_{LH,D}$ (kJ)
H_2O-LiCl	(4) 2.07×10^7	(1) 9.99×10^6	(4) 2.33×10^6	(5) 1.31×10^6
H_2O-LiBr	(5) 2.04×10^7	(2) 1.13×10^7	(5) 2.42×10^6	(4) 4.04×10^4
NH_3-$LiNO_3$	(1) 2.13×10^7	(3) 1.81×10^7	(1) 2.14×10^6	(1) 0.0
NH_3-NaSCN	(3) 2.08×10^7	(4) 1.89×10^7	(3) 2.31×10^6	(1) 0.0
NH_3-H_2O	(2) 2.09×10^7	(5) 2.10×10^7	(2) 2.26×10^6	(1) 0.0

The H_2O-LiCl and H_2O-LiBr systems obtained the minimum consumption of heating energy (9.99×10^6 kJ and 1.13×10^7 kJ, respectively), while the NH_3-H_2O system obtained the maximum value (2.10×10^7 kJ) because these systems can operate at a lower generator temperature than the NH_3-H_2O system.

The lost energy was caused mainly by the storage tank. The NH_3-$LiNO_3$ system obtained the lowest value of lost energy in the storage tank (2.14×10^6 kJ) and H_2O-LiBr obtained the highest (2.42×10^6 kJ), caused by the highest storage tank temperature. The lost energy due to the dissipating system was only activated for the H_2O-LiCl and H_2O-LiBr systems.

Figures 11 and 12 show the effect volume and the thickness of the insulator of the storage tank on the solar and heating fraction, respectively. The increment of the tank volume slightly lowers the values of SF, which positively affects the HF values.
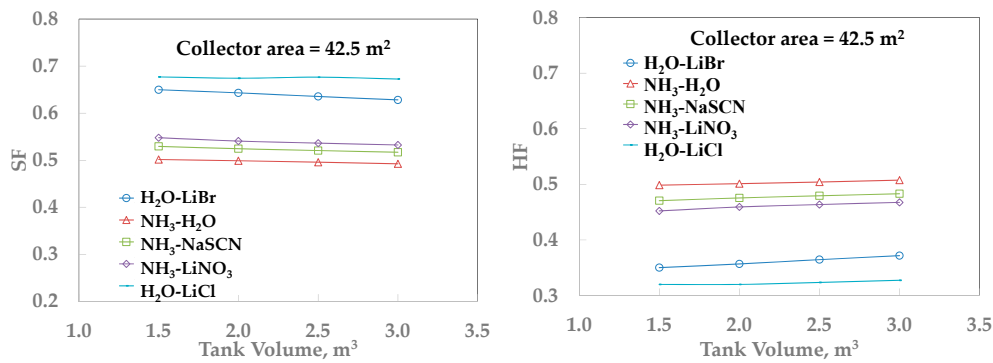
Figure 11. The energy fraction as a function of the volume tank using different working mixtures.
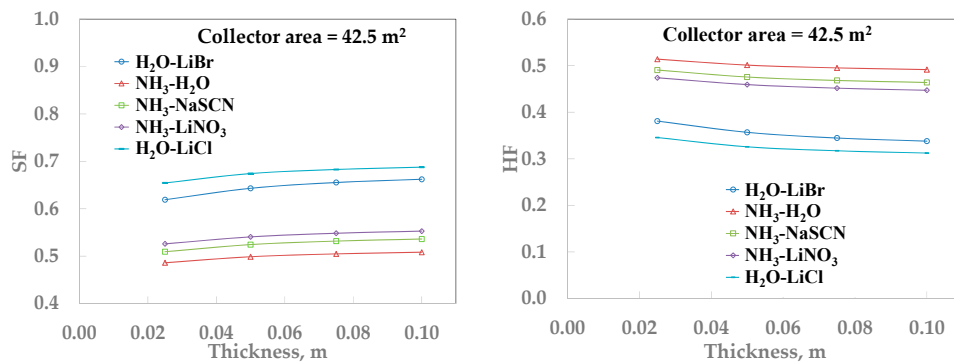

Figure 12. The energy fraction as a function of the insulation thickness of the storage tank.

The increment of the insulation thickness of the tank positively affects the solar fraction and negatively affects the heating fraction. Moreover, when the insulation thickness was higher than 0.08 m, the energy fractions were slightly affected by it.

Figure 13 shows that the increments of the solar collector area, the solar and lost heat fraction increase too. The maximum SF obtained was around 0.90 for the H_2O-LiBr and H_2O-LiCl systems using 77.20 m^2 of collector area and was 0.94 for the other working mixtures using 108.1 m^2 of collector area. After these values, the increment of the solar collector area will affect softly to the SF because the dissipation heat system is activated to avoid crystallization problems or COP values lower than 0.4 and because the generator temperature was limited to 135 °C.
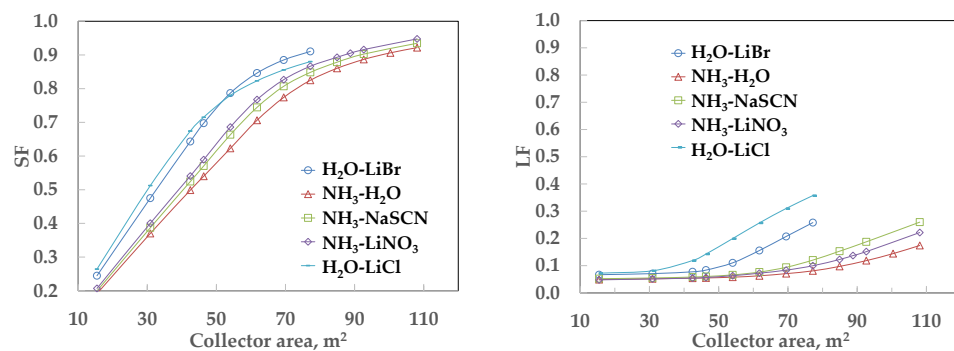

Figure 13. The energy fraction as a function of the number of solar collectors using different working mixtures.

The solar fraction shows a linear behavior from 15 to 50 m^2 of collector area for all working mixtures, after which the increment shows a logarithmic behavior because the energy lost (LF) starts

to increase due to the dissipation system. In order to select the adequate number of solar collectors for each working mixture, a maximization of the gain fraction (GF) parameter was carried out. This parameter represents the best relationship between the solar energy and the energy that is "not desirable" (the heating system and lost heat from the storage tank and dissipation system). Each working system obtained a maximum value of GF of 2.3, 3.8, 4.7, 6.1 and 6.6 for the H_2O-LiCl, H_2O-LiBr, NH_3-NaSCN, NH_3-H_2O and NH_3-LiNO$_3$ systems, respectively as is shown in Figure 14. Table 6 shows the number of solar collectors for each working mixture system and the energy fractions based on the GF. The H_2O-LiCl system obtained the minimum solar collector area (54.0 m^2), however, it obtained the maximum lost heat fraction (0.20) and the lowest solar fraction value (0.78). It was caused by the short working operation due to the crystallization problem. Meanwhile, the NH_3-LiNO$_3$ and NH_3-H_2O systems obtained the maximum solar (0.91) and minimum heating (0.09) fraction, using an area solar collector of 88.8 and 100.4 m^2, respectively. This means that this system could operate at a higher solar collector number with low lost energy.
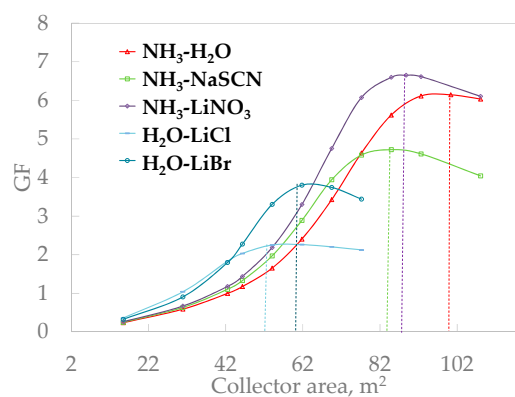

Figure 14. The gain fraction as a function of the number of solar collectors using different working mixtures.

Table 6. Results of energy fractions.

Working Mixture	GF	No. of Solar Collector	Solar Collector Area (m^2)	SF	HF	LF
H_2O-LiCl	2.3	14	54.0	0.78	0.22	0.20
H_2O-LiBr	3.8	16	61.8	0.85	0.15	0.16
NH_3-NaSCN	4.7	17	84.9	0.88	0.12	0.15
NH_3-H_2O	6.1	26	100.4	0.91	0.09	0.14
NH_3-LiNO$_3$	6.6	23	88.8	0.91	0.09	0.14

7. Conclusions

This paper presented a thermal analysis of the absorption cooling system with different working mixtures in a dynamic condition for conditioning a building located in Temixco, Mexico using TRNSYS and EES software. In this study, we analyzed the behavior of the system as a function of the number of evacuated solar collectors and the volume of the storage tank. The following conclusions are presented:

- The COP of the absorption cooling system analyzed the condenser and absorber temperatures at 30 and 44 °C at a fixed evaporator temperature of 8 °C, in order to select the operation range of the generator temperature to avoid obtaining values lower than 0.4 for the COP and crystallization zone, after which different condenser and absorber temperature ranges were set.
- A solar collector area of 42.5 m^2 was selected to carry out the thermal analysis because it presented the adequate relationship between the energy fraction of the heating system and the solar collectors. The H_2O-LiCl system obtained the maximum solar fraction (0.67) and the minimum heating fraction (0.33); however, it obtained the maximum lost heat fraction (0.12), in spite of obtaining the best COP among the other working mixtures. The NH_3-LiNO$_3$ system

obtained the maximum value of energy from solar collectors (2.13×10^7 kJ) and the H_2O-LiBr system was the worst (2.04×10^7 kJ) because it obtained a better COP than the NH_3-$LiNO_3$ system. Therefore, the storage tank temperature starts to increase, reducing the solar collector efficiency.

- The increment of the tank volume decreases the values of SF slightly, which positively affects the HF values. On the other hand, the increment of the insulation thickness of the tank positively affects the solar fraction and negatively affects the heating fraction. Moreover, when the insulation thickness was higher than 0.08 m, the energy fractions were slightly affected by it.

- The maximum solar fraction obtained was around 0.90 for the H_2O-LiBr and H_2O-LiCl systems using 77.20 m^2 of collector area and was 0.94 for the other working mixtures using 108.1 m^2 of collector area. This is because the dissipation heat system was activated to avoid crystallization problems or COP values lower than 0.4 and because the generator temperature was limited to 135 °C.

- A gains fraction was used to select the adequate solar collector number for each working mixture. This parameter represents the energy fraction between the solar collectors and the heating system and lost heat. The H_2O-LiCl system obtained the minimum GF (2.3), with a solar collector area of 54.0 m^2 (14 solar collectors). It was caused by a short working operation resulting from the crystallization problem. On the other hand, NH_3-$LiNO_3$ and NH_3-H_2O obtained the highest GF (up 6), both obtained the maximum solar (0.91) and minimum heating (0.09) fractions, respectively, using 88.8 and 100.4 m^2 of the solar collector area, respectively.

Author Contributions: Rosenberg Romero, Antonio Rodriguez and Jonathan Ibarra Bahena carried out the mathematical model of the ACS for all working mixtures in EES software and Jesus Cerezo, Alexis Acuña and Gisela Montero carried out the simulation of the solar absorption cooling system in TRNSYS software.

Conflicts of Interest: The authors declare no conflict of interest.

Nomenclature

A	area, m^2
ACS	absorption cooling system
AS	auxiliary system
COP	coefficient of performance, adim
C_p	heat capacity, kJ/kg °C
m	mass flow rate, kg/s
Q	heat load, kW
Qt	total energy, kJ
SC	solar collector
SHX	solution heat exchanger
T	temperature, °C
t	time, s
U	loss coefficient between the tank and its environment, kW/m^2 °C
h	specific enthalpy, kJ/kg
x	liquid ammonia concentration, % by weight
y	vapor ammonia concentration, % by weight

Subscripts

AB	absorber
CO	condenser
COOL	cooling
DH	dissipating system
ENV	environment
GE	generator
HS	heating system
HS	heating system
IN	input
LH	lost heat
OUT	output
RAD	radiation
SC	solar collector

Symbols

η	efficiency
α	control function for solar collector circuit
β	control function for cooling circuit

Appendix A.

This section describes the mathematical model of the single stage absorption cooling system to evaluate the coefficient of performance for each working mixture as well as its validation.

Appendix A.1. Simulation Model

The ACS (Figure 1b) simulation was based on simple mass and energy balances for each component [19] programmed in the EES software. The suppositions are described as follows:

1. The system operates under steady-state conditions.
2. The pressure drops and heat losses are negligible for each component and pipeline.
3. Expansion valves are adiabatic and isenthalpic.
4. The efficiency (ES_{HX}) of the solution heat exchanger (SHX) is 0.8.
5. The saturated condition at the condenser, evaporator, generator and absorber outlets.
6. The vapor (Point 5 from Figure 1) and solution (3) streams have the same temperature at the generator outlet.
7. The refrigerant is considered pure in the evaporator.
8. The power of the pump is negligible.

Appendix A.2. Energy Balances

Absorber

$$m_1 = m_4 + m_8 \tag{A1}$$

$$m_1\, x_1 = m_4\, x_4 + m_8\, y_8 \tag{A2}$$

$$m_1\, h_1 + Q_{AB} = m_4\, h_4 + m_8\, h_8 \tag{A3}$$

Generator

$$m_2 = m_3 + m_5 \tag{A4}$$

$$m_2\, x_2 = m_3\, x_3 + m_5\, y_5 \tag{A5}$$

$$m_2\, h_2 + Q_{GE} = m_3\, h_3 + m_5\, h_5 \tag{A6}$$

Condensador

$$m_5 = m_6 \tag{A7}$$

$$m_5\, h_5 = m_6\, h_6 + Q_{CO} \tag{A8}$$

Evaporador

$$M_7 = m_8 \tag{A9}$$

$$M_7\, h_7 + Q_{EV} = m_8\, h_8 \tag{A10}$$

Economizer (SHX)

$$Q_{MAX1} = m_1\, C_{p,1}\, (T_3 - T_1) \tag{A11}$$

$$Q_{MAX3} = m_3\ C_{p,3}\ (T_3 - T_1) \tag{A12}$$

$$Q_{MIN} = MIN(Q_{MAX3}, Q_{MAX5}) \tag{A13}$$

$$Q_{SHX} = ES_{HX}\ Q_{MIN} \tag{A14}$$

$$h_2 = Q_{SHX}/m_1 + h_1 \tag{A15}$$

$$h_4 = h_3 - Q_{SHX}/m_3 \tag{A16}$$

$$m_1\ h_1 + m_3\ h_3 = m_4\ h_4 + m_2\ h_2 \tag{A17}$$

Coefficient of performance

$$COP = \frac{Q_{EV}}{Q_{GE}}$$

Appendix A.3. Validation

The COP obtained from the CAS simulation were compared with simulations reported by different authors for each working mixture.

Appendix A.3.1. H_2O-LiBr System

The H_2O-LiBr thermodynamic properties were obtained from the publication of Patek and Klomfar [20] programed as a library routine in the EES software. The COP obtained in this study was compared with that of the Gogoi and Konwar [13] simulation at different temperatures conditions as shown in Table A1. The COP difference percent was lower than 2.6% between the present simulation and the bibliography.

Table A1. Simulation results of the H_2O-LiBr absorption cooling system.

T_{EV}, °C	T_{GE}, °C	T_{CO}, °C	T_{AB}, °C	COP [13]	COP, Author	Difference, %
4	70	31	31	0.79	0.79	0.9
5	66	28	35	0.77	0.76	0.8
6	72	33	37	0.73	0.73	0.5
8	85	46	39	0.58	0.60	−2.6
9	66	28	34	0.84	0.83	0.7

Appendix A.3.2. H_2O-LiCl System

The H_2O-LiCl thermodynamic properties were obtained from the publication of Patek and Klomfar [21] (heat capacity) and Conde [22] (concentration, density, and enthalpy). The COP obtained in this study was compared with that of the Gogoi and Konwar [13] simulation at different temperatures conditions as shown in Table A2. The COP difference percent was lower than 10% between the present simulation and the bibliography.

Table A2. Simulation results of the H_2O-LiCl absorption cooling system.

T_{EV}, °C	T_{GE}, °C	T_{CO}, °C	T_{AB}, °C	COP [13]	COP, Author	Difference %
4	70	31	31	0.86	0.82	3.6
5	66	28	35	0.86	0.82	4.8
6	72	33	37	0.84	0.79	5.7
8	85	46	39	0.81	0.73	10.0
9	66	28	34	0.85	0.86	2.7

Appendix A.3.3. NH_3-$LiNO_3$ System

The NH_3-$LiNO_3$ thermodynamic properties were obtained from the publication of Infante Ferreira [23]. Table A3 shows the values of COP obtained from the Sun simulation [12] and from the present work at an evaporator temperature = −5 °C and condenser and absorber = 25 °C. The COP difference percent is lower than 8%.

Table A3. Simulation results of the NH$_3$-LiNO$_3$ absorption cooling system.

T$_{GE}$,°C	COP [12]	COP, Author	Difference %
60	0.52	0.54	3.4
65	0.60	0.65	7.7
75	0.64	0.67	5.5
85	0.64	0.67	4.5
95	0.64	0.65	2.6

Appendix A.3.4. NH$_3$-NaSCN System

The NH$_3$-NaSCN thermodynamic properties were obtained from the publication of Ferreira [23]. Table A4 shows the values of COP obtained from the Sun simulation [12] and the present work at an evaporator temperature = −5 °C and condenser and absorber = 25 °C. The COP difference percent is lower than 8%.

Table A4. Simulation results of the NH$_3$-NaSCN absorption cooling system.

T$_{GE}$, °C	COP [12]	COP, Author	Difference %
65	0.53	0.55	3.99
75	0.62	0.65	4.29
85	0.63	0.66	4.70
95	0.63	0.66	3.21

Appendix A.3.5. NH$_3$-H$_2$O System

The NH$_3$-H$_2$O thermodynamic properties were obtained from the publication of Ibrahim and Klein [24] programmed as an EES Library routine in the EES software. Table A5 shows the values of COP obtained from the Sun simulation [12] and the present work at an evaporator temperature = −5 °C and condenser and absorber = 25 °C. The COP difference percent is lower than 13%.

Table A5. Simulation results of the NH$_3$-H$_2$O absorption cooling system.

T$_{GE}$, °C	COP [12]	COP, Author	Difference %
65	0.54	0.56	3.90
75	0.62	0.63	1.21
85	0.62	0.62	0.26
100	0.62	0.60	4.67
120	0.62	0.54	12.75

References

1. Gilania, S.I.; Ahmed, M.S. Solution crystallization detection for double-effect LiBr-H$_2$O steam absorption chiller. *Energy Procedia* **2015**, *75*, 1522–1528. [CrossRef]
2. Ahmed, M.S.; Waheed, A.; Talha, T.; Wajahat, M.; Sarfraz, F. Configuration based modeling and performance analysis of single effect solar absorption cooling system in TRNSYS. *Energy Convers. Manag.* **2018**, *157*, 351–363.
3. Stanciu, C.; Stanciu, D.; Gheorghian, A.T. Thermal analysis of a solar powered absorption cooling system with fully mixed thermal storage at startup. *Energies* **2017**, *10*, 72. [CrossRef]
4. Stanciu, C.; Stanciu, D.; Gheorghian, A.-T.; Tănase, E.-B.; Dobre, C.; Spiroiu, M. Maximum exergetic efficiency operation of a solar powered H$_2$O-LiBr absorption cooling system. *Entropy* **2017**, *19*, 676. [CrossRef]
5. Sokhansefat, T.; Mohammadi, D.; Kasaeian, A.; Mahmoudi, A.R. Simulation and parametric study of a 5-ton solar absorption cooling system in Tehran. *Energy Convers. Manag.* **2017**, *148*, 339–351. [CrossRef]
6. Antonopoulos, K.A.; Rogdakis, E.D. Performance of solar-driven ammonia-lithium nitrate and ammonia-sodium thiocyanate absorption systems operating as coolers or heat pumps in Athens. *Appl. Therm. Eng.* **1996**, *16*, 127–147. [CrossRef]
7. Florides, G.A.; Kalogirou, S.A.; Tassou, S.A.; Wrobel, L.C. Modelling and simulation of an absorption solar cooling system for Cyprus. *Sol. Energy* **2002**, *72*, 43–51. [CrossRef]

8. Arzoz, D.; Venegas, M.; Izquierdo, M.; Rodríguez, P. Solar absorption refrigeration cycle using $LiNO_3$-NH_3 solution and flat plate collectors. In Proceedings of the International Sorption Heat Pump Conference, Shangai, China, 24–27 September 2002.

9. De Francisco, A.; Illanes, R.; Tones, J.L.; Castillo, M.; De Bias, M.; Prieto, E.; García, A. Development and testing of a prototype of low power water-ammonia absorption equipment for solar energy applications. Renew. *Energy* **2002**, *25*, 537–544.

10. Asim, M.; Dewsbury, J.; Kanana, S. TRNSYS simulation of a solar cooling system for the hot climate of Pakistan. *Energy Procedia* **2016**, *91*, 702–706. [CrossRef]

11. Agrouaza, Y.; Bouhal, T.; Allouhi, A.; Kousksou, T.; Jamil, A.; Zeraouli, Y. Energy and parametric analysis of solar absorption cooling systems in various Moroccan climates. *Case Stud. Therm. Eng.* **2017**, *9*, 28–39. [CrossRef]

12. Sun, D.W. Comparison of the performances of NH_3-H_2O, NH_3-$LiNO_3$ and NH_3-NaSCN absorption refrigeration systems. *Energy Convers. Manag.* **1998**, *39*, 357–368. [CrossRef]

13. Gogoi, T.K.; Konwar, D. Exergy analysis of a H_2O-LiCl absorption refrigeration system with operating temperatures estimated through inverse analysis. *Energy Convers. Manag.* **2016**, *110*, 436–447. [CrossRef]

14. Solar Energy Laboratory. TRNSYS 18, a Transient System Simulation Program. Available online: http://sel.me.wisc.edu/trnsys (accessed on 21 January 2018).

15. Klein SA. *EES, Engineering Equation Solver*; Professional Version; FChart Software: Madison, WI, USA, 2017; Available online: http://www.fchart.com/ees/ (accessed on 21 January 2018).

16. Solar Rating & Certification Corporation. *Directory of SRCC Certified Solar Collector Ratings*; Solar Rating & Certification Corporation: Washington, DC, USA, 2009.

17. Solar Energy Laboratory. TRNSYS 17 mathematical reference. In *Available under the TRNSYS 17 Help Menu*; Solar Energy Laboratory: Madison, WI, USA, 2017.

18. Klein, S.A. EES Engineering Equation Solver, User Manual, F-Chart Software. Available online: http://www.unh.edu/p2/ihf/ees.pdf (accessed on 1 November 2018).

19. Cerezo, J. Study of Absorption Process with Ammonia-Water Using Plate Heat Exchanger for Absorption Refrigeration Machines. Ph.D. Thesis, Universitat Rovira i Virgili, Tarragona, Cataluña, Spain, 2006. (In Spanish)

20. Patek, J.; Klomfar, J. A computationally effective formulation of the thermodynamic properties of LiBr-H_2O from 273 to 500 K over full composition range. *Int. J. Refrig.* **2006**, *29*, 566–578. [CrossRef]

21. Patek, J.; Klomfar, J. Thermodynamic properties of the LiCl-H_2O system at vapor–liquid equilibrium from 273 K to 400 K. *Int. J. Refrig.* **2008**, *31*, 287–303. [CrossRef]

22. Conde, M. Aqueous Solution of Lithium and Calcium Chlorides: Property Formulations for Use in Air Conditioning Equipment Design. 2014. Available online: www.mrc-eng.com/Downloads/Aqueous%20LiCl&CaCl2%20Solution%20Props.pdf (accessed on 20 January 2018).

23. Infante-Ferreira, C.A. Thermodynamic and physical property data equations for ammonia-lithium nitrate and ammonia-sodium thiocyanate solutions. *Sol. Energy* **1984**, *32*, 231–236. [CrossRef]

24. Ibrahim, O.M.; Klein, S.A. Thermodynamic Properties of Ammonia—Water Mixtures, ASHRAE. *Transactions* **1993**, *99*, 1495–1502.